

# The projected isotropic normal distribution with applications in neuroscience

Kanti V. Mardia<sup>1</sup> and Antonio Mauricio F.L. Miranda de Sá<sup>2</sup>

<sup>1</sup> Department of Statistics, University of Leeds, Woodhouse, Leeds LS2 9JT, UK; k.v.mardia@leeds.ac.uk

<sup>2</sup> Biomedical Engineering Program, Federal University of Rio de Janeiro, Brazil; amflms@peb.ufrj.br

## Abstract

This paper is motivated by a cutting-edge application in neuroscience: the analysis of electroencephalogram (EEG) signals recorded under flash stimulation. Under commonly used signal-processing assumptions, only the phase angle of the EEG is required for the analysis of such applications. We demonstrate that these assumptions imply that the phase has a projected isotropic normal distribution. We revisit this distribution and derive several new properties, including closed-form expressions for its trigonometric moments. We then examine the distribution of the mean resultant and its square — a statistic of central importance in phase-based EEG studies. The distribution of the resultant is analytically intricate; to make it practically useful, we develop two approximations based on the well-known resultant distribution for the von Mises distribution. We then study inference problems for this projected isotropic normal distribution. The method is illustrated with an application to EEG data from flash-stimulation experiments.

**Keywords:** component synchrony measure, EEG, phase angle, resultant, score matching approximation, von Mises distribution

## 1 Introduction

Our paper is motivated by a cutting-edge application in biomedical signal analysis, which deals with analysing biomedical signals. These signals are collected from the body at the organ, cellular, or molecular level. There are different biomedical signals, including the electroencephalogram (EEG), which reflects electrical activity from

the brain, and the electrocardiogram (ECG), which reflects electrical activity from the heart, among others (see, for example, Muthuswamy (2004), Subasi (2019), and Anand et al. (2022)). ECG traces are well-known (as used for the heart). Mushtaq et al. (2024), in reviewing one hundred years of EEG research, emphasise the importance of methodological progress by stating that “Future work should aim to develop EEG pipelines that are transparent, reproducible and generalizable across populations and contexts.” This call for improved workflows implicitly includes the adoption of new statistical tools and analytical frameworks capable of handling the complexity and variability inherent in EEG data.

The EEG signals are, in general, univariate time series (Muthuswamy and Thakor, 1998). The Fourier transform of such a series provides a quantitative description of its frequency content. For neurological data, examining spectral or frequency-domain characteristics is often as important as studying time-domain behaviour. For example, changes in electroencephalograms (EEGs) across different stages of sleep are more clearly captured through frequency-domain features. Although our application focuses on EEG responses to flash stimulation (Section 8), the same principles apply across a wide range of experimental paradigms.

**Model.** To formalise this framework, we treat EEG recordings as traces or univariate continuous-time series  $x(t)$ , where  $t \in \mathbb{R}^+$  (the non-negative real line), typically regarded as defined on  $0 \leq t < \infty$ .

Under some plausible assumptions, Miranda de Sá et al. (2002) and Miranda de Sá and Felix (2003) have proposed that the discrete Fourier transform  $Y_j$  of  $x(t)$  at frequency  $j$  can be modelled as

$$Y_j = \mu + e_{1j} + i e_{2j}, \quad j = 1, 2, \dots, \quad (1.1)$$

where  $i = \sqrt{-1}$ , and  $e_{1j}$  and  $e_{2j}$  are independent error terms. Further, it has been shown in various studies that, for EEG applications like ours, the *phase* of the Fourier transform plays the main role rather than its magnitude (Busch et al., 2009; Busch and VanRullen, 2010; Mathewson et al., 2009; Notbohm and Herrmann, 2016). That is, only the angular component  $\theta$  of  $Y_j$  in (1.1) is of interest. Although the joint model (1.1) was proposed by Miranda de Sá et al. (2002) and Miranda de Sá and Felix (2003), it was not recognised that the resulting phase distribution belongs to the family of projected normal distributions (see, for example, Mardia and Jupp (2000)). In Section 2, we derive this distribution for our setting and refer to it as the projected isotropic normal (PIN) distribution. In Section 3, we obtain population moments of the PIN distribution and use these to construct two approximations by the von Mises distribution: the standard approximation and a new approximation based on the score-matching method.

The well-known summary statistic “mean resultant”  $\bar{R}$  in directional statistics is found to capture the behaviour of the phase of the Fourier transform (see Section 4). In the biomedical literature, its square ( $\bar{R}^2$ ) is also used and termed the “Component Synchrony Measure (CSM)”. To perform statistical inference on CSM, we need the sampling distribution of the resultant length  $R$  under the PIN distribution, which is

considered in Section 4.2. It is seen that the distribution is complicated, but it can be approximated using the distribution under the von Mises case. For small and large values of the concentration parameter of the PIN distribution, both approximations are very good, and even for mid-range values the loss is minimal (see Sections 4 and 5).

In Section 6, we consider estimation of the parameters, including the maximum likelihood method; the maximum likelihood estimates can be obtained only using numerical methods, and we provide some approximate closed-form estimates, including those based on the score-matching method. Under a deterministic response to stimulation, the phase would be identical across trials, and the noise component would have a uniform phase distribution. Thus, the phase itself becomes the crucial quantity for formulating the null hypothesis of no response. In Section 7, we consider hypothesis testing under the PIN distribution and provide confidence intervals for CSM. In Section 8, we then apply these results to biomedical EEG signals recorded under flash stimulation. Finally, Section 9 highlights the key contributions of the paper and gives directions for further work. Some supplementary material has been given in Appendices ; Appendix 1 A examines the EEG model in detail; Appendix 2 B gives the proof of moments formula for the PIN distribution and Appendix 3 C examines further the two approximations to the PIN distribution by the von Mises distribution.

## 2 The Projected Isotropic Normal (PIN) distribution

Let  $(x_1, x_2)^T$  be distributed as an isotropic bivariate normal distribution with mean vector  $(\mu_1, \mu_2)^T$  and covariance matrix  $\sigma^2 \mathbf{I}$  where  $\mathbf{I}$  is the identity matrix. Let

$$x_1 = r \cos \theta, \quad x_2 = r \sin \theta, \quad r > 0, \quad 0 \leq \theta \leq 2\pi, \quad (2.1)$$

then  $\theta$ , in terms of the Fourier transform model, is the *phase angle*. This distribution of  $\theta$  is a particular case of the general projected normal distribution given in Mardia (1972), page 92, equation (3.4.17), under a bivariate normal with general mean vector and general covariance matrix. To deduce the projected normal distribution for our case, in that equation we substitute

$$\mu = \mu_1 = \beta \cos \mu, \quad \nu = \mu_2 = \beta \sin \mu, \quad \sigma_1^2 = \sigma_2^2 = \sigma^2, \quad \rho = 0, \quad (2.2)$$

which leads to the following form of the projected normal distribution, where  $\gamma = \beta^2/(4\sigma^2)$ .

**Definition 1.** *The Projected Isotropic Normal (PIN) distribution of  $\theta$  has the following probability density function (pdf):*

$$f(\theta; \mu, \gamma) = \frac{1}{2\pi} \exp(-2\gamma) + 2\sqrt{\gamma} \cos(\theta - \mu) \Phi(2\sqrt{\gamma} \cos(\theta - \mu)) \phi(2\sqrt{\gamma} \sin(\theta - \mu)), \quad (2.3)$$

where  $-\pi \leq \theta \leq \pi$ ,  $\gamma \geq 0$ , and  $\gamma$  is the “concentration parameter” of the PIN distribution. We say that  $\theta$  is distributed as  $PIN(\mu, \gamma)$ , or simply  $PIN(\gamma)$  if  $\mu = 0$ .

We sometimes write

$$SNR = 2\gamma, \gamma = \frac{1}{2} SNR, \quad (2.4)$$

where SNR stands for “Signal-to-Noise Ratio”, defined already in Section 1.

We note that projected normal distributions are well established (see, for example, Mardia and Jupp (2000)). The distribution for the circular case in general was given by Mardia (1972), with some particular cases. Note that for the circular case it is also called the off-set normal distribution by Mardia and Jupp (2000), the displaced normal by Kendall (1974), and the angular normal by Watson (1983).

In practice, the von Mises distribution, the wrapped normal distribution, and the PIN distribution can each qualify as a “circular normal”. Each has its own merits; for example, the PIN and wrapped normal distributions are the easiest to simulate, while for testing uniformity the von Mises distribution leads to the Rayleigh test. Note that all three can be derived from the bivariate normal or the univariate normal: the von Mises distribution is the conditional distribution of  $\theta$  given  $r$  in  $(r, \theta)$ , the PIN distribution is the marginal distribution of  $\theta$  in  $(r, \theta)$ , and the wrapped normal distribution is obtained by wrapping the univariate normal distribution.

It is not surprising that all three have been compared using the moment estimator of the concentration parameter (with  $\mu = 0$  without any loss of generality), starting from Kendall (1974). Watson (1983) (and recently summarised by Presnell et al. (1998)) made a thorough comparison and concluded that the maximum difference occurs at  $\rho = .785$  ( $\kappa = 2.7$ ,  $\gamma = 0.64$ ), where  $\rho$  denotes the population resultant. Section 3.1 studies further the PIN distribution approximated by a von Mises distribution.

We now give some properties of the PIN distribution. As  $\gamma \rightarrow \infty$ ,  $\Phi(2\sqrt{\gamma} \cos \theta) \rightarrow 1$ , so from (2.3) we obtain

$$f(\theta; \gamma) \propto \sqrt{\gamma} |\cos \theta| \exp(-2\gamma \sin^2 \theta) d\theta, \quad (2.5)$$

that is,

$$f(\theta) \propto \exp(-2\gamma\theta^2), \quad (2.6)$$

so  $\theta$  is distributed as  $N(0, 1/(4\gamma))$ , which would mean that  $4\gamma = 2 SNR$  is the concentration parameter, although we take  $\gamma$  as our concentration parameter. It can be seen that

$$f(-\theta; \gamma) = f(\theta; \gamma),$$

so the distribution is symmetrical about  $\theta = 0$ . Further, let  $2\sqrt{\gamma} = \delta$ . Then the derivative of  $f(\theta; \gamma)$  with respect to  $\theta$  is

$$-2\delta \sin \theta [(1 + \delta) \Phi(\delta \cos \theta) \phi(\delta \sin \theta) + \delta^2 \cos^2 \theta \Phi(\delta \cos \theta)].$$

Since the terms in square brackets are positive, the mode can be verified to be at  $\theta = 0$ . The value of the pdf at the mode is

$$\frac{1}{2\pi} \exp(-2\gamma) + \sqrt{2\gamma/\pi} \Phi(2\sqrt{\gamma}),$$

and the antimode at  $\theta = \pi$  is

$$\frac{1}{2\pi} \exp(-2\gamma) - \sqrt{2\gamma/\pi} \Phi(2\sqrt{\gamma}).$$

**Simulation.** It is straightforward to simulate a sample from the PIN distribution. Most statistical software includes a routine to simulate a normal distribution, so we can draw a sample from

$$x_1 \sim N(\mu_1, \sigma^2), \quad x_2 \sim N(\mu_2, \sigma^2),$$

and obtain the sample value of  $\theta$  from (2.1). We note that, since we are starting from a bivariate normal distribution, a simple method to simulate is via the well-known Box–Muller transformation.

### 3 Population Moments and the von Mises Approximations

We now obtain the trigonometric moments of the PIN distribution, which will be used below to obtain approximations of the PIN distribution by a von Mises distribution. We assume, without any loss of generality, that the mean direction is zero for both distributions. It can be shown, after some tedious algebra, that the following hold:

$$E(\sin \theta) = 0, \quad E(\sin 2\theta) = 0, \quad E(\cos \theta) = \sqrt{\pi\gamma/2} \exp(-\gamma) \{I_0(\gamma) + I_1(\gamma)\}, \quad (3.1)$$

where  $I_p(\cdot)$  is the modified Bessel function of the first kind and of order  $p$ , given by

$$I_p(z) = \sum_{m=0}^{\infty} \frac{(\frac{1}{4}z^2)^{m+\frac{p}{2}}}{m! \Gamma(p+m+1)}. \quad (3.2)$$

This result was first stated in Kendall (1974). Further, the population resultant  $\rho$  is simply  $E(\cos \theta)$ ; note that here  $E(\cos \theta) \geq 0$ . We also have  $E(\cos \theta \sin \theta) = \frac{1}{2}E(\sin 2\theta) = 0$  (see below).

In fact, we extend the above results to higher moments, and the results are as follows.

**Theorem 2.**

$$E(\sin p\theta) = 0, \quad (3.3)$$

$$E(\cos p\theta) = \sqrt{\pi\gamma/2} \exp(-\gamma) \{I_{(p-1)/2}(\gamma) + I_{(p+1)/2}(\gamma)\}. \quad (3.4)$$

where  $p$  is an integer.

A proof is given in Appendix 2.

Note that for even moments, (3.4) can be simplified as follows. With  $p = 2k$ , using Abramowitz and Stegun (1964), Equation (10.2.4), p. 445, we have

$$\sqrt{\pi\gamma/2} I_{k+1/2}(\gamma) = \gamma^k \left( \frac{1}{\gamma} \frac{d}{d\gamma} \right)^k \frac{\sinh \gamma}{\gamma}.$$

Using this expression for  $k = 0, 1$  in (3.4) with  $p = 2$ , it can be shown that

$$E(\cos 2\theta) = 1 - \frac{\exp(-\gamma)}{\gamma} \sinh \gamma. \quad (3.5)$$

It is interesting that, in this case, this second cosine moment is simpler than the first cosine moment given by (3.1).

### 3.1 The von Mises Approximations

On the circle, the von Mises distribution (like the normal distribution) has two parameters, with the pdf of the angle  $\theta$  given by

$$f(\theta; \mu, \kappa) = \frac{\exp\{\kappa \cos(\theta - \mu)\}}{2\pi I_0(\kappa)}, \quad 0 \leq \theta < 2\pi, \quad (3.6)$$

where  $\mu$  is the mean direction,  $0 \leq \mu < 2\pi$ , and  $\kappa$  is the concentration (“inverse variance”) parameter,  $\kappa \geq 0$ , with  $I_0(\kappa)$  the modified Bessel function of the first kind and order zero given in (3.2). This distribution is symmetrical with mode at  $\mu$ . For  $\kappa = 0$ ,  $\theta$  is uniformly distributed on the circle. For large  $\kappa$ ,  $\theta$  is approximately normal with mean  $\mu$  and variance  $2/\kappa$ . We denote this distribution by  $\text{vM}(\mu, \kappa)$ , and when  $\mu = 0$  we denote the distribution by  $\text{vM}(\kappa)$ .

We now show how to approximate the PIN distribution  $\text{PIN}(\gamma)$  by the von Mises distribution  $\text{vM}(\kappa)$ , with concentration parameter  $\kappa$ .

#### 3.1.1 The Standard von Mises Approximation: Approx 1

The standard approximation consists of equating the moment  $E(\cos \theta)$  of the two distributions. That is,

$$A(\kappa) = \sqrt{\pi\gamma/2} \exp(-\gamma) \{I_0(\gamma) + I_1(\gamma)\} \quad \text{or} \quad \kappa = A^{-1} \left( \sqrt{\pi\gamma/2} \exp(-\gamma) \{I_0(\gamma) + I_1(\gamma)\} \right), \quad (3.7)$$

where  $A(\kappa) = I_1(\kappa)/I_0(\kappa)$  and  $I_p(\cdot)$  denotes the modified Bessel function of the first kind and order  $p$  given in (3.2). We refer to the approximation defined by (3.7) as Approx 1.

From (3.7), it is shown below that

$$\text{for small } \kappa \text{ or for small } \gamma, \quad \kappa = \sqrt{2\pi\gamma}, \quad (3.8)$$

whereas

$$\text{for large } \kappa \text{ or for large } \gamma, \quad \kappa = 4\gamma. \quad (3.9)$$

To derive these small- and large- $\kappa$  expressions for Approx 1, we use standard expansions for the modified Bessel functions of the first kind, as given in Appendix 1 of Mardia and Jupp (2000). We substitute into (3.7) the following approximations and the proof follows:

$$\text{For small } \kappa : \quad I_0(\kappa) \approx 1, \quad I_1(\kappa) \approx \kappa. \quad (3.10)$$

$$\text{For large } \kappa : \quad I_0(\kappa) \approx \frac{\exp(\kappa)}{\sqrt{2\pi\kappa}} \left(1 + \frac{1}{8\kappa}\right), \quad I_1(\kappa) \approx \frac{\exp(\kappa)}{\sqrt{2\pi\kappa}} \left(1 - \frac{3}{8\kappa}\right). \quad (3.11)$$

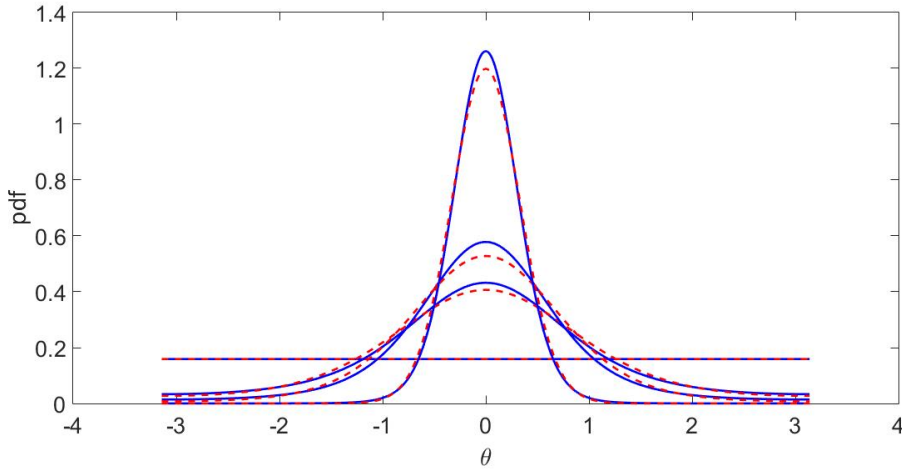


Figure 1: . Projected isotropic normal (PIN) distribution for different values of  $\gamma$  (0, 0.25, 0.5, 2.5) shown in continuous blue lines, and the corresponding von Mises distribution approximation (Approx 1) shown in dashed red lines.

### 3.1.2 Score Matching von Mises Approximation: Approx 2

We now derive the Score Matching Approximation (SMA) as developed in Mardia (2017) and Mardia (2018). From Mardia (2017),

$$\kappa = \frac{2E(\cos \theta)}{1 - E(\cos 2\theta)}. \quad (3.12)$$

In Mardia (2018), the same equation (equation (19)) contains a typo: in the right-hand side of this equation, the factor 2 should be deleted, and the same correction applies to the particular cases given in (20) and (21).

On substituting  $E(\cos \theta)$  from (3.1) and  $E(\cos 2\theta)$  from (3.5) into (3.12), we obtain our second approximation:

$$\kappa = \frac{\gamma\sqrt{2\pi\gamma}\{I_0(\gamma) + I_1(\gamma)\}}{\sinh \gamma}. \quad (3.13)$$

We refer to this approximation defined by (3.13) as Approx 2. From (3.13), we show that

$$\text{for small } \kappa \text{ or for small } \gamma, \quad \kappa = \sqrt{2\pi\gamma}, \quad (3.14)$$

and further,

$$\text{for large } \kappa \text{ or for large } \gamma, \quad \kappa = 4\gamma. \quad (3.15)$$

To derive thees small- and large- $\kappa$  expressions we again use some standard expansions for the modified Bessel functions of the first kind, as given in Appendix 1 of Mardia and Jupp (2000). We substitute into (3.13):

- For small  $\kappa$ , use (3.10) and  $(\sinh \gamma)/\gamma \approx 1$ . - For large  $\kappa$ , use (3.11) and  $\sinh \gamma \approx \exp(\gamma)/2$ .

Comparing (3.8)–(3.9) with (3.14)–(3.15) shows that Approx 1 and Approx 2 are identical in both the small- and large- $\kappa$  cases.

We note that Approx 2 is simpler than Approx 1, since in Approx 2 the left-hand side of equation (3.13) does not involve any Bessel function (cf. (3.7)). However, we have found that their overall performance is similar when applied to problems involving the PIN distribution; these details are given in Appendix 3 C . Mostly, we will concentrate on Approx 1, except when we need the computational advantage of Approx 2.

## 4 Distribution of the Mean Resultant

Let  $\theta_1, \dots, \theta_n$  be a random sample drawn from  $\text{PIN}(\gamma)$ , and let us write

$$\bar{C} = \frac{1}{n} \sum_{i=1}^n \cos \theta_i, \quad \bar{S} = \frac{1}{n} \sum_{i=1}^n \sin \theta_i, \quad (4.1)$$

Then the sample mean resultant  $\bar{R}$  is given by

$$\bar{R} = \sqrt{\bar{C}^2 + \bar{S}^2}. \quad (4.2)$$

We now give the different nomenclature used in the EEG literature for the mean resultant, to highlight its target application. We start with the term used for  $\bar{R}^2$ .

**Definition 3.** *The quantity  $\bar{R}^2$  is the “component synchrony measure” (CSM) of the output signal, denoted by  $\hat{\rho}^2(f)$ . CSM is also known as “phase synchrony” or “phase synchrony measure”; see, for example, Friedman et al. (1984).*

That is,

$$\text{CSM} = \bar{R}^2 = \bar{C}^2 + \bar{S}^2 = R^2/n^2 = \hat{\rho}^2(f), \quad (4.3)$$

where  $f$  in  $\hat{\rho}^2(f)$  highlights that these quantities arise from the frequencies of the EEG trace. In psychology, synchrony refers to the spontaneous rhythmic coordination of actions, emotions, thoughts, and physiological processes across time between two or more individuals.

Furthermore, the mean resultant appears with terminology specific to EEG data in Cohen (2014) as follows: the Phase Locking Value (PLV) is the name used for the mean resultant. In particular, the term Inter-Site Phase Clustering (ISPC) (Cohen (2014), Chapter 19) is used for PLV computed for a single electrode site, whereas the same term is also used for PLV computed from phase-angle differences for two electrode sites. ‘‘Clustering’’ here is synonymous with concentration.

Our aim is to obtain the distribution of  $\bar{R}$  under the PIN distribution. We start with asymptotics, recalling that it is uniform when  $\gamma = 0$ .

## 4.1 Asymptotics

It is well-known that under uniformity, for large  $n$ , we have (see, for example, Mardia and Jupp (2000), page 77)

$$2n\bar{R}^2 \asymp \chi_2^2. \quad (4.4)$$

This result depends on the fact that  $(\bar{C}, \bar{S})$  are asymptotically independent normals with means 0 and variances  $1/(2n)$ . Note that in this uniform case, the exact pdf can be written down; see Section 4.2 below. In general, we have from Mardia and Jupp (2000), page 76, the asymptotic distribution of  $\bar{R}$  as a normal distribution. In fact, from page 76 of Mardia and Jupp (2000), we find that in our case, for large  $n$ ,  $(\bar{C}, \bar{S})$  are asymptotically independent normals with means and variances as follows:

$$E(\bar{C}) = \alpha, \quad E(\bar{S}) = 0, \quad \text{var}(\bar{C}) = \frac{1}{2n}(1 + \alpha_2), \quad \text{var}(\bar{S}) = \frac{1}{2n}(1 - \alpha_2), \quad (4.5)$$

where  $\alpha = E(\cos \theta)$  and  $\alpha_2 = E(\cos 2\theta)$ .

Note that using (4.4), it can be shown that for large  $n$  we have

$$E(\bar{R}) = \sqrt{\frac{\pi}{4n}}, \quad E(\bar{R}^2) = \frac{1}{n}, \quad \text{var}(\bar{R}) = \frac{1}{n} \left(1 - \frac{\pi}{4}\right), \quad \text{var}(\bar{R}^2) = \frac{1}{n^2}. \quad (4.6)$$

## 4.2 Distributions of the Resultant

Let  $R = n\bar{R}$ . The pdf of  $R$  under **uniformity** is (see Mardia and Jupp (2000), page 66)

$$h_n(R) = R \int_0^\infty u J_0(Ru) J_0(u)^n du, \quad (4.7)$$

where  $J_0(\cdot)$  denotes the Bessel function of the first kind and order zero. Also, we note that the pdf of  $R$  for **the von Mises case** with concentration parameter  $\kappa$  is given by (see Mardia and Jupp (2000), page 69)

$$p(R) = \frac{I_0(\kappa R)}{I_0(\kappa)^n} h_n(R), \quad 0 < R < n, \quad (4.8)$$

where  $h_n(R)$  is given by (4.7). Hence, using the simple transformation (4.3) from  $R$  to  $v = \bar{R}^2 = R^2/n^2$  ( $v = \text{CSM} = \hat{\rho}^2(f)$ ), the distribution of  $v$  under the von Mises distribution is

$$p(v) = \frac{n^2}{2} \frac{I_0(n\kappa\sqrt{v})}{I_0(\kappa)^n} \int_0^\infty u J_0(n\sqrt{v}u) J_0(u)^n du, \quad 0 < v < 1. \quad (4.9)$$

Note that for  $\kappa \geq 4$ , a very good approximation to the distribution of  $R$  for the von Mises case (4.9) is given by Stephens (1969):

$$2n\gamma^*(1 - \bar{R}) \sim \chi_{n-1}^2, \quad (4.10)$$

where

$$\frac{1}{\gamma^*} = \frac{1}{\kappa} + \frac{3}{8\kappa^2}. \quad (4.11)$$

Further, the percentage points of this distribution for the von Mises case are given in Stephens (1969).

## 5 The CSM Distribution and von Mises Approximations

In the last section, we gave an explicit expression for the sampling distribution of  $R$  (or CSM) under the von Mises population, but the exact sampling distribution under the PIN distribution is not tractable, as we indicate even for the simplest case  $n = 2$ . The distribution of the resultant length  $R$  from Kent et al. (1979) for  $n = 2$ , with a sample from a population with pdf  $f(\cdot)$  (the CSM is a function of  $R$ ), is given from Equation (2.4) as

$$\frac{4 \int_0^{2\pi} f(u-t)f(u+t) du}{(4 - R^2)^{1/2}}, \quad 0 < R < 2, \quad (5.1)$$

where  $t = \arccos(R/2)$ . It can be shown that for the von Mises case, this expression simplifies to (4.8) for  $n = 2$ , noting that

$$h_2(R) = \frac{2}{\pi(4 - R^2)^{1/2}}, \quad 0 < R < 2. \quad (5.2)$$

However, even for this simplest case, (5.6) cannot be simplified for the PIN distribution. As a practical solution, we now assume that Approx 1 provides the pdf of CSM for given

values of  $\gamma$  under the PIN distribution by plugging in the value of  $\kappa$  corresponding to  $\gamma$  from Approx 1 into (4.9) for  $\gamma > 0$ ,

$$p(v; \gamma) = \frac{n^2}{2} \frac{I_0(n\kappa(\gamma)\sqrt{v})}{I_0(\kappa(\gamma))^n} \int_0^\infty u J_0(nu\sqrt{v}) J_0(u)^n du, \quad 0 < v < 1, \gamma > 0, \quad (5.3)$$

where

$$\kappa(\gamma) = A^{-1} \left( \sqrt{\pi\gamma/2} \exp(-\gamma) \{I_0(\gamma) + I_1(\gamma)\} \right),$$

and using (4.4) for  $\gamma = 0$

$$p(v; \gamma = 0) = 2 \int_0^\infty u J_0(u\sqrt{v}) J_0(u)^n du. \quad (5.4)$$

To assess this approximation, we simulated the distribution of CSM (or  $R$ ) from the distribution of  $\theta$  under the PIN distribution. Simulation of  $\theta$  is straightforward: given  $\gamma$ , draw two independent normal variables

$$x = r \cos \theta \sim N(\sqrt{4\gamma}, 1), \quad y = r \sin \theta \sim N(0, 1),$$

and compute  $\theta = \arctan 2(y, x)$  (the function  $\arctan 2$  returns the correct quadrant, so  $0 \leq \theta \leq 2\pi$ ). We used  $n = 10$  and 100,000 simulations for  $\gamma = 0, 0.25, 0.5, 2.5$ , with the corresponding  $\kappa$  values from Approx 1: (0, 1.4, 2.1, 9.3). Figure 2 shows the simulated CSM histograms from the PIN density (blue, shaded), together with the approximate CSM density (red, solid outline) provided by Approx 1, equation (4.9). It can be seen that the approximation is very good for small and large values of  $\gamma$ , and acceptable for the mid-range. Note that we selected  $n = 10$  as such low values are common in EEG stimulation studies (see also Section 8 with  $n = 12$ .) **Remark** In EGG, if we allow the time dependent between observations, the distribution of the resultant length  $R$  even for  $n=2$  will be influenced by dependence. Let us assume for the angles on torus  $(\theta_1, \theta_2)$  have the Mardia's cosine distribution (Mardia (1975a), Mardia (1975b))

$$f(\theta_1, \theta_2) = \frac{1}{(2\pi)^2 I_0(\lambda)} \exp \{ \lambda \cos(\theta_1 - \theta_2) \} \quad (5.5)$$

where the association parameter  $\lambda > 0$  favours  $\theta_1 \approx \theta_2$  and hence larger  $R$ , while  $\lambda < 0$  favours  $\theta_1 \approx \theta_2 + \pi$  and shifts mass towards smaller  $R$ . Note that the resultant for  $n=2$  of the two angles  $\theta_1$  and  $\theta_2$  can be seen to

$$R = 2|\cos(\theta_1 - \theta_2)/2|.$$

Now from Kent et al. (1979) for  $n = 2$ , with a sample from a population with pdf  $f(\cdot)$  (the CSM is a function of  $R$ ), can be extended from Equation (2.4) to as

$$\frac{4 \int_0^{2\pi} f(u-t, u+t) du}{(4-R^2)^{1/2}}, \quad 0 < R < 2, \quad (5.6)$$

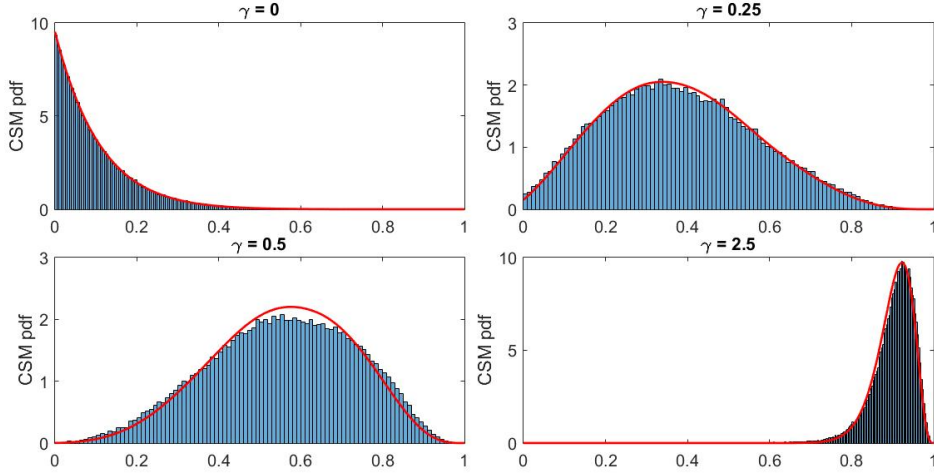


Figure 2: Simulated CSM histograms for  $\gamma = 0, 0.25, 0.5, 2.5$  from the PIN density (blue, shaded), with the density (5.3) of CSM (red solid outline) obtained using Approx 1.

where  $t = \arccos(R/2)$ . It can be shown that for the cosine von Mises case, this cosine expression simplifies for  $n = 2$  to,

$$f(R) = \frac{2I_0(2\lambda \arccos(R/2))}{\pi I_0(\lambda)(4 - R^2)^{1/2}}, \quad 0 < R < 2. \quad (5.7)$$

For  $\lambda \rightarrow 0$ , it reduces to the uniform distribution case given at (5.2).

## 6 Estimation

Let  $\theta_i$ ,  $i = 1, \dots, n$  be a random sample from the PIN distribution. Then the maximum likelihood estimates (mles)  $\hat{\mu}$ ,  $\hat{\gamma}$  of  $\mu$ ,  $\gamma$  are obtained by solving the (log-)likelihood equation from (2.3):

$$\log L(\gamma) = \sum \log f(\theta_i; \mu, \gamma). \quad (6.1)$$

However, this expression cannot be simplified so the mles  $\hat{\mu}$ ,  $\hat{\gamma}$  must be computed numerically. We now give some approximation procedures.

**Hybrid Estimates.** Let

$$\bar{C} = \bar{R} \cos \bar{\theta}, \quad \bar{S} = \bar{R} \sin \bar{\theta}, \quad (6.2)$$

where  $\bar{\theta}$  is the sample mean direction. One procedure is to plug into (6.1)

$$\mu = \bar{\theta}, \quad (6.3)$$

and then maximise the function with respect to  $\gamma$ , leading to the hybrid estimate  $\hat{\gamma}_{\text{HYB}}$ .

**Moment Estimators.** Let us write

$$E(\sin \theta) = \rho \sin \mu, \quad E(\cos \theta) = \rho \cos \mu, \quad (6.4)$$

where  $\rho$  is now a function of  $\gamma$ , written as  $\rho(\gamma)$ . For  $\mu$ , we take the sample mean direction as a moment estimator:

$$\hat{\mu}_{\text{MOM}} = \bar{\theta}.$$

The simplest moment estimator of  $\rho$  is

$$\hat{\rho}_{\text{MOM}} = \bar{R}, \quad (6.5)$$

which leads to a moment estimator  $\hat{\gamma}_{\text{MOM}}$  of  $\gamma$  by substituting the value of  $\rho$  from (3.1):

$$\bar{R} = \sqrt{\pi\gamma/2} \exp(-\gamma) \{I_0(\gamma) + I_1(\gamma)\}. \quad (6.6)$$

It can be shown that

$$\text{for small } \gamma, \quad \hat{\gamma}_{\text{MOM}} = \frac{2\bar{R}^2}{\pi}, \quad (6.7)$$

whereas

$$\text{for large } \gamma, \quad \hat{\gamma}_{\text{MOM}} = \frac{1}{8(1 - \bar{R})}. \quad (6.8)$$

Approx 2 provides another ‘‘moment’’ estimate of  $\gamma$  by using, for the von Mises distribution,  $A(\hat{\kappa}) = \bar{R}$  in Approx 2. Thus  $\hat{\gamma}_{\text{MOM2}}$  is the solution of

$$\bar{R} = A\left(\frac{\sqrt{2\pi\gamma} \{I_0(\gamma) + I_1(\gamma)\}}{(\sinh \gamma)/\gamma}\right). \quad (6.9)$$

**MLE of CSM.** In some applications, we need to obtain the mle of the population CSM  $\rho^2$ . Using the expression for  $\rho$  from (3.1), the mle  $\hat{\rho}_{\text{MLE}}^2$  of  $\rho^2$  is

$$\hat{\rho}_{\text{MLE}}^2 = (\pi\hat{\gamma}/2) \exp(-2\hat{\gamma}) \{I_0(\hat{\gamma}) + I_1(\hat{\gamma})\}^2. \quad (6.10)$$

**Bias.** We can study the bias in the approximate mles of  $\gamma$  via well-known results for the von Mises case related to  $\kappa$ . The estimator  $\hat{\kappa} = A^{-1}(\bar{R})$  can be heavily biased for  $n \leq 15$ , and a modified estimator  $\hat{\kappa}^*$  is given by (see, for example, Fisher (1993), Mardia and Jupp (2000))

$$\hat{\kappa}^* = \begin{cases} \max\{\hat{\kappa} - 2(n\hat{\kappa})^{-1}, 0\}, & \hat{\kappa} < 2, \\ \frac{(n-1)^3 \hat{\kappa}}{n^3 + n}, & \text{otherwise.} \end{cases} \quad (6.11)$$

**Asymptotic Distribution of  $\hat{\gamma}$ .** Since our main focus is on the concentration parameter  $\gamma$  rather than  $\mu$ , we consider only the asymptotic distribution of its estimator  $\hat{\gamma}$ . For large  $n$ ,

$$\hat{\gamma} \sim N(\gamma, 1/(nI)),$$

where  $I$  is the Fisher information,

$$I = E \left[ \frac{\partial^2}{\partial \gamma^2} \log L(\gamma) \right],$$

and  $\log L(\gamma)$  is given by (6.1). There is no analytical simplification of  $I$ , so we resort to approximations. In fact, we can show that

$$\hat{\gamma}_{\text{MOM}} \sim N \left( \gamma, \frac{1}{n \text{var}(\hat{\gamma}_{\text{MOM}})} \right),$$

where  $\text{var}(\hat{\gamma}_{\text{MOM}})$  is derived as follows. Let  $\hat{\rho} = \bar{R}$ . From a Taylor approximation,

$$\text{var}(\hat{\gamma}_{\text{MOM}}) = \left( \frac{d\rho}{d\gamma} \right)^2 \text{var}(\hat{\rho}). \quad (6.12)$$

It can be shown from (6.4) and standard relations for the Bessel functions  $I_0(\gamma)$  and  $I_1(\gamma)$  that

$$\frac{d\rho}{d\gamma} = \sqrt{\frac{\pi}{2\gamma}} \frac{\exp(-\gamma)}{2I_0(\gamma)} \{1 - A(\gamma)\}. \quad (6.13)$$

Hence,

$$\text{var}(\hat{\gamma}_{\text{MOM}}) = \frac{\pi}{8\gamma} \frac{\exp(-2\gamma)}{I_0(\gamma)^2} \{1 - A(\gamma)\}^2 \text{var}(\bar{R}). \quad (6.14)$$

We now quote the following asymptotic variance expressions for  $\bar{R}$  in the von Mises case so that Approx 1 can be used. For large  $\kappa$ , from (4.8.31) of Mardia and Jupp (2000),

$$\text{var}_1(\bar{R}) = \frac{1}{2n\kappa^2}, \quad (6.15)$$

whereas for large  $n$ , from (4.8.18),

$$\text{var}_2(\bar{R}) = \frac{1}{n} \left\{ 1 - A(\kappa)^2 - \frac{A(\kappa)}{\kappa} \right\}. \quad (6.16)$$

Thus we obtain two asymptotic expressions for  $\text{var}(\hat{\gamma})$  by substituting either  $\text{var}_1(\bar{R})$  from (6.15) or  $\text{var}_2(\bar{R})$  from (6.16) into (6.14), depending on the values of  $\kappa$  and  $n$ .

For CSM,

$$\hat{\rho}_{\text{MOM}}^2 \sim N \left( \rho^2, \frac{2}{n \text{var}(\bar{R})} \right),$$

and again we may substitute either  $\text{var}_1(\bar{R})$  or  $\text{var}_2(\bar{R})$ .

We now report some experiments showing that the mle is unique and examine the performance of the mle approximations.

## 6.1 Numerical experiments

**Uniqueness of the MLE of  $\gamma$ .** To investigate the uniqueness and accuracy of the maximum likelihood estimator  $\hat{\gamma}$ , we performed a simulation study. For each true value  $\gamma \in \{0.5, 1, 1.5, 2, 3\}$  we generated samples of size  $n = 10$  from the PIN model and computed the log-likelihood  $\log L(\gamma)$  (see 6.1 ). Figure 3 displays the log-likelihood curves for these settings. Each curve is unimodal and the mode lies very close to the true value of  $\gamma$ , supporting the practical uniqueness of the MLE in these cases.

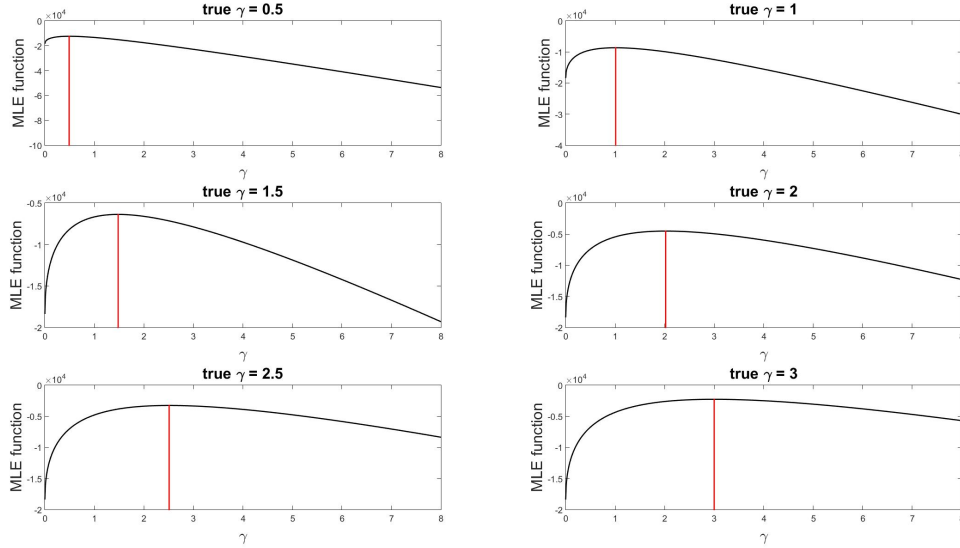


Figure 3: Log-likelihood (6.1) for samples of size  $n = 10$  drawn from the PIN distribution with  $\gamma = 0.5, 1, 1.5, 2, 2.5, 3$ . Red vertical lines indicate the modes of the respective curves.

**MLE with approximations.** We compared Approx 1 and Approx 2 to the MLE of across  $\rho^2$  (CSM) for a range of SNR ( $=2\gamma$ ) values and sample sizes  $n = 10, 100, 1000$ . Figure 4 shows estimates of  $\rho^2$  (CSM) obtained from Approx 1 (blue), Approx 2 (red), and the MLE (black). Both approximations perform well overall, but their relative accuracy depends on  $n$  and the SNR which we now summarize.

- For large  $n$  (e.g.,  $n = 1000$ ), Approx 1 closely matches the MLE across the SNR range.
- For small  $n$  (e.g.,  $n = 10$ ) and low-to-moderate SNR, Approx 2 is slightly closer to the MLE.
- In practice the two approximations are similar for most SNR values; differences are most noticeable in the mid-range SNR and for small sample sizes.

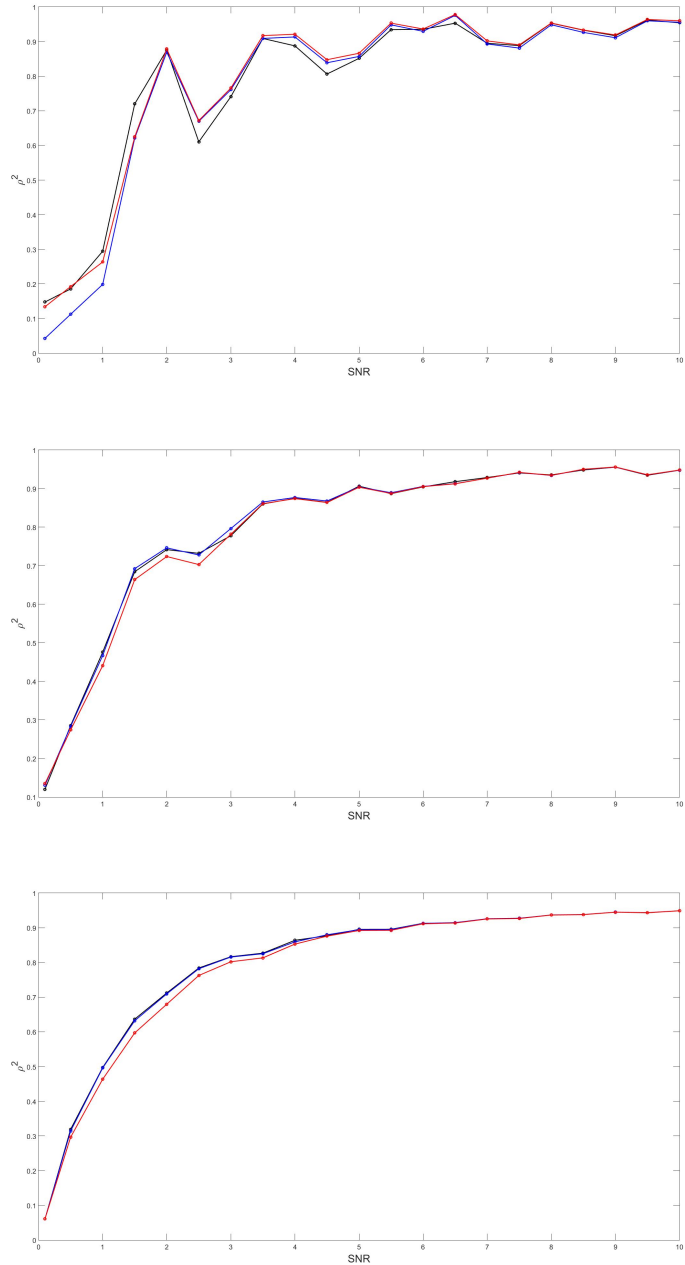


Figure 4: Estimates of  $\rho^2$  against SNR ( $=2\gamma$ ) using Approx 1 (blue), Approx 2 (red), and the MLE (black) for sample sizes  $n = 10$  (top),  $n = 100$  (middle), and  $n = 1000$  (bottom).

For routine applications with moderate to large sample sizes, Approx 1 is convenient and more accurate. When sample sizes are small and SNR is in the mid range, Approx 2 provides a modest improvement. When the highest possible accuracy is required (for example, when making inference in the tails of the distribution), the MLE remains the preferred choice.

## 7 Hypothesis Testing and Confidence Intervals

**Testing of Hypotheses.** Let  $\theta$  be distributed as  $\text{PIN}(\mu, \gamma)$  and let  $\theta_i, i = 1, \dots, n$  be a random sample drawn from this distribution. We want to test the null hypothesis  $H_0$  of uniformity against a simple alternative:

$$H_0 : \gamma = 0 \quad \text{vs} \quad H_1 : \gamma = \gamma_1.$$

We can write the log-likelihood ratio (LRT) from (2.3) as

$$-n \log(2\pi) + \sum \log f(\theta_i; \mu, \gamma_1). \quad (7.1)$$

For a composite alternative with  $\mu$  unknown,

$$H_0 : \gamma = 0 \quad \text{vs} \quad H_1 : \gamma \neq 0,$$

the log-likelihood ratio is

$$-n \log(2\pi) + \sum \log f(\theta_i; \hat{\mu}, \hat{\gamma}), \quad (7.2)$$

where  $\hat{\mu}$  and  $\hat{\gamma}$  are the maximum likelihood estimates described in Section 6. We cannot simplify the LRT statistics in (7.1) and (7.2); for data, they must be computed numerically.

One way to partially overcome this difficulty is to use a von Mises approximation. For the von Mises case, the LRT test in (7.2) reduces to the Rayleigh test, which is uniformly most powerful (see, for example, Mardia and Jupp (2000)). The test is

$$\text{reject } H_0 \quad \text{for large values of } \bar{R}. \quad (7.3)$$

Tables for the von Mises case are available (see Stephens (1969)). For large  $n$ , we may use the approximation in (4.4); the statistic has a chi-square distribution with 2 degrees of freedom (i.e., an exponential distribution), and the critical value is

$$\bar{R}_{\text{crit}}^2 = \frac{\ln(1/\alpha)}{n}.$$

For use in Section 8, note that for  $\alpha = 0.05$  and  $n = 12$ , we have  $\bar{R}_{\text{crit}}^2 = 0.25$  (as used in Figure 7). From Stephens (1969), the exact 5% value of  $\bar{R}$  is 0.494, so  $\bar{R}^2 = 0.244$ , showing that the approximation is good even for  $n = 12$ .

Also, for large  $n$ ,

$$E(\bar{R}^2) = \frac{1}{n}, \quad \text{var}(\bar{R}^2) = \frac{1}{n^2},$$

leading to the simpler approximation

$$(n\bar{R}^2 - 1) \sim N(0, 1). \quad (7.4)$$

For 5% significance and  $n = 12$ , this approximation gives  $\bar{R}^2 = 0.247$ , which is slightly better in this case.

Indeed, we can carry out inference for the PIN distribution approximately (especially for large  $n$ ) using Approx 1 or Approx 2 by using the corresponding von Mises solution. This includes confidence intervals for  $\gamma$  via  $\kappa$ , and other inferential procedures, which we now describe. More examples appear in the application section.

**Confidence Intervals.** Let us consider confidence intervals for  $\gamma$  by using the confidence intervals for  $\kappa$  given in Mardia and Jupp (2000), pp. 150–151, and then applying one of our approximations as described below.

1. For  $\kappa \geq 2$  (equivalently,  $\gamma \geq 0.5$ ), an approximate  $(1 - \alpha)$  confidence interval for  $\kappa$  is

$$(\kappa_l, \kappa_u), \quad \kappa_l = \frac{1 + \sqrt{1 + 3a}}{4a}, \quad \kappa_u = \frac{1 + \sqrt{1 + 3b}}{4b}, \quad (7.5)$$

with

$$a = \frac{n - R}{\chi_{n-1; 1-\alpha/2}^2}, \quad b = \frac{n - R}{\chi_{n-1; \alpha/2}^2}, \quad (7.6)$$

where  $\chi_{n-1; \alpha/2}^2$  denotes the upper  $\alpha/2$  point of the  $\chi_{n-1}^2$  distribution.

For example, using  $\kappa = 4\gamma$  for large  $\gamma$  (from Approx 1 or Approx 2), we obtain an approximate  $(1 - \alpha)$  confidence interval for  $\gamma$  from (7.5):

$$\frac{1}{4}\kappa_l \leq \gamma \leq \frac{1}{4}\kappa_u, \quad (7.7)$$

where  $\kappa_l$  and  $\kappa_u$  are given by (7.5) in terms of  $R$ .

2. For  $\kappa < 2$  (equivalently,  $\gamma < 0.5$ ), we may use the bootstrap (see Fisher (1993), pp. 88–92). Before constructing a confidence interval, however, we should first test the null hypothesis of uniformity,  $\kappa = 0$ . If the null is accepted, a confidence interval for  $\kappa$  is not relevant.

Note that for  $\kappa = 2$ , we have  $\rho = 0.698$  and  $\rho^2 = 0.487$ , i.e.,  $\rho^2 \approx 0.5$  to one decimal place. Thus, if we observe  $\bar{R}^2 \geq 0.5$ , we may use the confidence interval for  $\gamma$  given in (7.7).

## 8 Applications to Biomedical Signals: EEG Stimulation Study

We present an illustrative example of biomedical signals consisting of electroencephalogram (EEG) recordings during a visual type of stimulation called intermittent photic stimulation (IPS). We first describe how the EEG trace data are acquired. In general,

electrodes are placed on the scalp according to standardized positions, as shown in Figure 5, which displays the common 10–20 international EEG system. According to convention, the letters indicate the anatomical regions beneath the electrode: O (occipital), T (temporal), C (central), P (parietal), and F (frontal). Odd numbers denote electrodes in the left hemisphere and even numbers those in the right hemisphere.

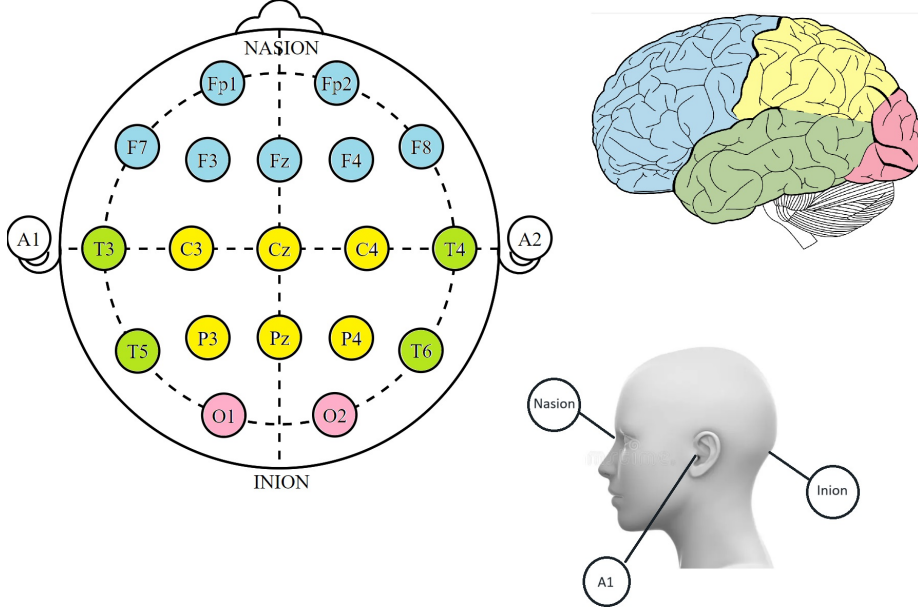


Figure 5: EEG electrode positions in the 10–20 international system. The electrode sites are shown in the same colours as the corresponding underlying lobes of the brain: F (frontal), C (central), P (parietal), O (occipital), and T (temporal). The head diagram indicates the locations of the fiducial points (nasion, left pre-auricular point, and inion).

The data used here were collected in Miranda de Sá et al. (2002). These consist of EEG recordings during IPS with stroboscopic light flashing at 6 Hz (six flashes per second) from a subject at two electrodes close to the visual cortex ( $O_1$  with O = occipital, and  $P_3$  with P = parietal; see Figure 5). The EEG was digitised using a 16-bit analogue-to-digital converter with a sampling frequency of 256 Hz. Each 1-second signal produced a time series of 256 points. The EEG time series for electrode  $O_1$  over 24 seconds is shown in Figure 6.

We split the time series into consecutive 2-second segments, yielding  $n = 12$  sub-time series, each with 512 points. Figure 6 displays the entire 24-second EEG record used for estimating the CSM. The discrete Fourier transform of each sub-series was computed using the fast Fourier transform (FFT) algorithm (each sub-series has  $2^9 = 512$  points). The phase of the Fourier transform was then extracted as required in our PIN model. Thus, at each frequency, we obtained 12 phase angles and computed the CSM from (4.3). Figure 7 shows the CSM for this dataset plotted against frequency (up to 36 Hz).

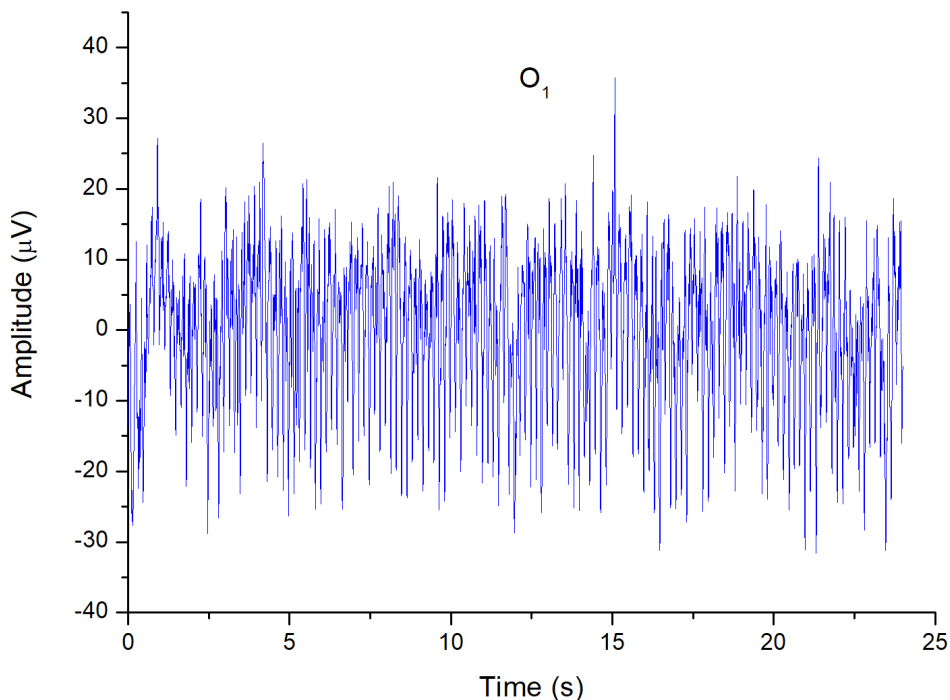


Figure 6: Time series of EEG recorded at electrode  $O_1$  for a subject stimulated at 6 Hz with stroboscopic flickering light. x-axis: time in seconds; y-axis: scaled voltage.

The horizontal dotted line marks the 95% critical value under uniformity, which from Section 7 is 0.25. The figure also shows the 95% confidence intervals at frequencies 6, 12, 18, 24, 30 Hz obtained from Section 7.

For comparison, we also present results for electrode  $P_3$ . Figure 8 shows the corresponding time series, and Figure 9 shows the CSM against frequency. Visually, the two CSM plots (Figures 7 and 9) differ markedly at the peaks, except at 12 Hz. As an illustration, we test the hypothesis of equality of the two concentration (SNR) parameters at frequency  $f = 6$  Hz. The data with  $n = 12$  are given in Table 1, and summary statistics appear in Table 2.

Table 1: Phase angles of  $O_1$  and  $P_3$  at 6 Hz,  $n = 12$

O1	-2.2032	-1.9798	-2.0625	-2.2151	-2.2389	-2.0569	-2.2505	-2.1924	-2.1404	-2.1541	-2.1244	-2.1647
P3	2.1879	-0.2305	-1.6763	-1.7409	-2.8771	-1.9322	2.9193	2.8651	-3.0499	-1.9783	3.0112	-2.7492

Let us assume that the samples for  $O_1$  and  $P_3$  come from  $\text{PIN}(\mu_1, \gamma_1)$  and  $\text{PIN}(\mu_2, \gamma_2)$ , respectively. First, we report using Section 6 that the hybrid estimates of  $\gamma_1$  and  $\gamma_2$  are 41.24 and 0.29, respectively, confirming that  $O_1$  is highly concentrated in comparison with  $P_3$ .

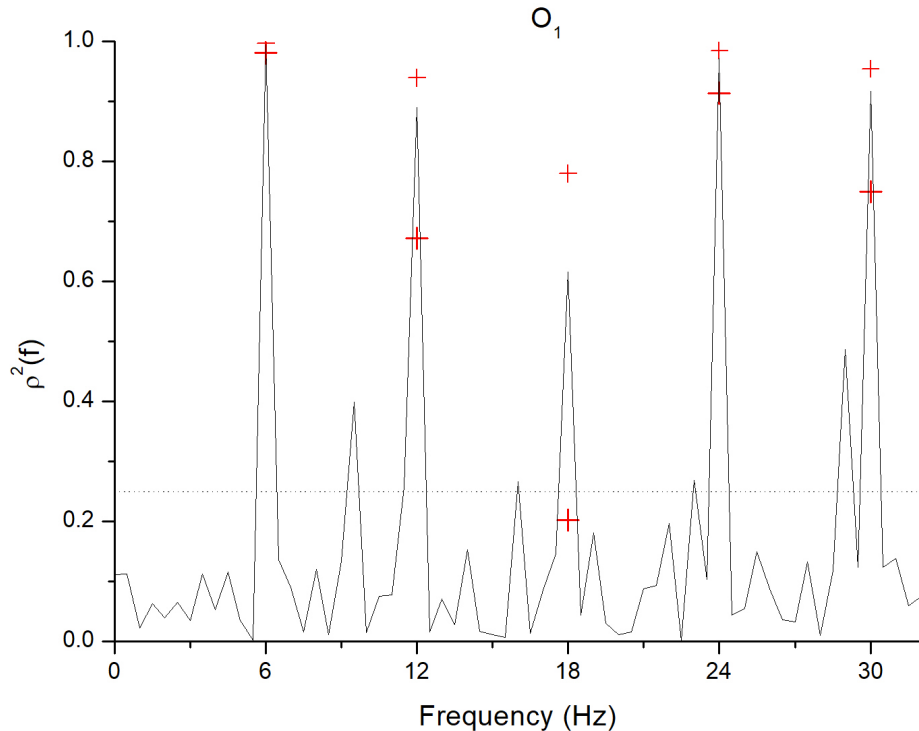


Figure 7: CSM for a subject stimulated at 6 Hz with stroboscopic flickering light at electrode  $O_1$ . The ‘+’ symbols indicate 95% confidence limits at the harmonics of stimulation. The horizontal dotted line indicates the critical value under uniformity ( $\bar{R}^2 = 0.25$ ,  $\bar{R} = 0.5$ ).

As an illustration, we now test the hypothesis

$$H_0 : \gamma_1 = \gamma_2 \quad \text{vs} \quad H_1 : \gamma_1 \neq \gamma_2.$$

Let  $\lambda$  be the likelihood ratio (Section 7) . We find  $-2 \log \lambda = 43.7$ , which is approximately  $\chi_2^2$  and therefore highly significant. Assuming a von Mises model, we have

$$F_{11,11} = \frac{1 - \bar{R}_2}{1 - \bar{R}_1} = 101,$$

again highly significant. Further, the 95% confidence interval for the CSM from (7.7) of Section 7 of  $O_1$  is (0.9810, 0.9967), and the 95% confidence interval for the CSM of  $P_3$  is (0.0507, 0.7652). This again confirms that  $O_1$  is highly concentrated, whereas  $P_3$  is much more diffuse.

Table 2: Summary statistics for the phase angle data of  $O_1$  and  $P_3$ ,  $n = 12$

Statistic	$O_1$	$P_3$	$O_1 + P_3$
$\bar{C}$	-0.5445	-0.5370	-0.5408
$\bar{S}$	-0.8351	-0.2799	-0.5575
$\bar{\theta}$	237°	208°	226°
$\bar{R}$	0.997	0.606	0.777
CSM	0.9939	0.3667	0.6037

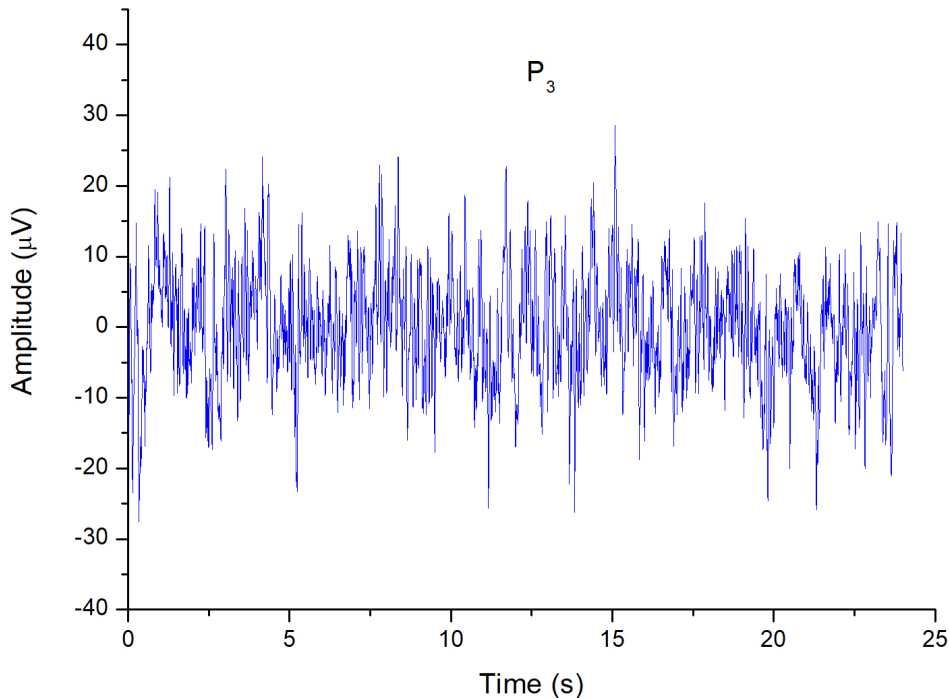


Figure 8: Time series of EEG recorded at electrode  $P_3$  for a subject stimulated at 6 Hz with stroboscopic flickering light, x-axis: time in seconds; y-axis: scaled voltage.

## 9 Discussion

In this paper, we have developed a phase-based framework for analysing EEG signals using the projected isotropic normal (PIN) distribution. Starting from the Fourier representation of EEG traces, we identified the phase as the key quantity for detecting stimulus-related responses and showed that its distribution arises naturally as a projected isotropic normal model. We derived population moments of the PIN distribution and proposed two von Mises approximations, both of which perform well across a wide range of concentration parameters. These results enabled practical inference for the Component Synchrony Measure (CSM), including confidence intervals and hypothesis

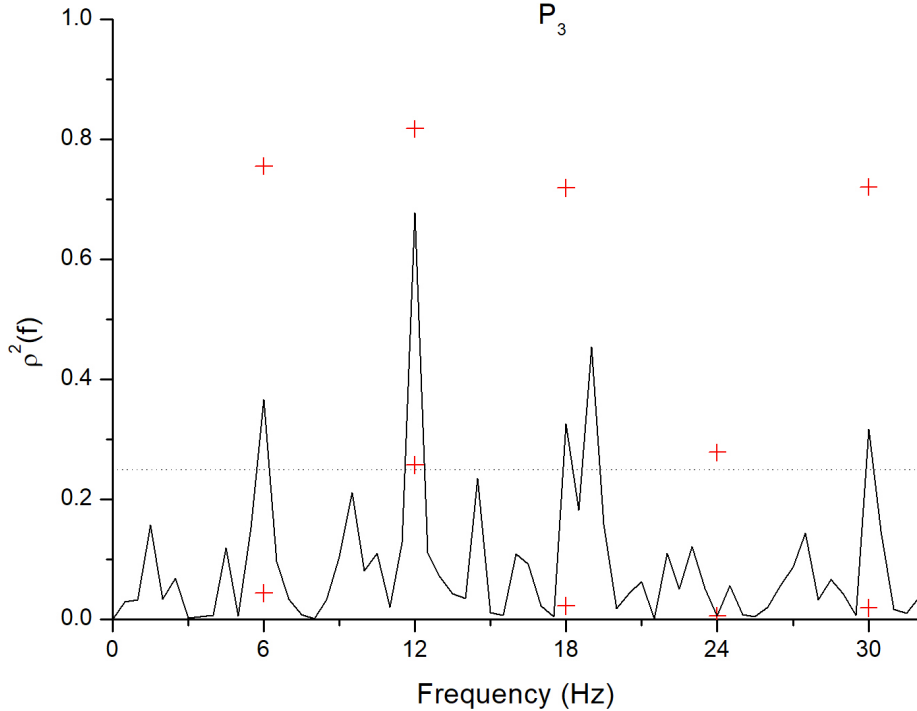


Figure 9: CSM for a subject stimulated at 6 Hz with stroboscopic flickering light at electrode  $P_3$ . The ‘+’ symbols indicate 95% confidence limits at the harmonics of stimulation. The horizontal dotted line indicates the critical values under uniformity ( $\bar{R}^2 = 0.25$ ,  $\bar{R} = 0.5$ ).

tests.

We provided estimation procedures for the model parameters, including approximate closed-form estimators and score-matching methods, and we developed testing procedures under the PIN framework, including tests for uniformity of phase and related hypotheses.

The application to EEG data under flash stimulation illustrated how the proposed methodology can be used in practice. These tools allow us to assess whether the observed phase distribution departs from uniformity, as would be expected under a stimulus-related response, and to compare synchrony across conditions using measures such as CSM.

The framework developed here opens several avenues for future work, particularly when moving beyond the single-electrode setting of our illustrative application. Although we treated the  $O_1$  and  $P_3$  samples as independent, they are of course correlated because they originate from the same subject. Joint modelling of multiple electrodes is therefore a natural next step. In such settings, the phase angles lie on a torus, and one extension

of the projected normal distribution to toroidal data is given by Kato et al. (1925). Moreover, EEG recordings exhibit spatial–temporal dependence across electrode sites, and methods for analysing such spatial–temporal data are discussed in Kent and Mardia (2022); these would be relevant for future developments of our approach.

Although our application focused on EEG data recorded under flash stimulation, phase-based analyses arise in many other experimental paradigms. For example, Busch et al. (2009) and Busch and VanRullen (2010) use the instantaneous phase of spontaneous EEG to study visual attention. This suggests that the PIN framework and the associated inference for CSM may be broadly applicable across cognitive and biomedical neuroscience.

For inference, an alternative to the classical approach adopted here is Bayesian analysis, following Nuñez-Antonio and Gutiérrez-Peña (2005). Such methods may be particularly useful when incorporating prior information or when modelling multiple electrodes simultaneously, and they offer a flexible direction for future work.

## 10 Acknowledgments

Kanti Mardia wishes to thank John Kent, Faisal Mushtaq, and Xiangyu Wu for their helpful comments.

## References

- Abramowitz, M. and Stegun, I. (1964) *Handbook of Mathematical Functions with Formulas, Graphs, and Mathematical Tables*. New York: United States Department of Commerce, National Bureau of Standards (NBS).
- Anand, S., Sharma, V., Pourush, R. and Jaiswal, S. (2022) A comprehensive survey on the biomedical signal processing methods for the detection of covid-19. *Annals of Medicine and Surgery*, **76**, 103519.
- Busch, N. A., Dubois, J. and VanRullen, R. (2009) The phase of ongoing eeg oscillations predicts visual perception. *The Journal of Neuroscience*, **29**, 7869–7876.
- Busch, N. A. and VanRullen, R. (2010) Spontaneous eeg oscillations reveal periodic sampling of visual attention. *Proceedings of the National Academy of Sciences of the United States of America*, **107**, 16048–16053.
- Cohen, M. X. (2014) *Analyzing Neural Time Series Data: Theory and Practice*. Cambridge, MA: MIT Press. URL: <https://mitpress.mit.edu/9780262019873/analyzing-neural-time-series-data/>.
- Fisher, N. I. (1993) *Statistical Analysis of Circular Data*. Cambridge University Press.

- Friedman, J., Zappulla, Bergelson, M., Greenblatt, E., Mails, L., Morrell, F. and Hoepfner, T. (1984) Application of phase spectral analysis for brain stem auditory evoked potential detection in normal subjects and patients with posterior fossa tumors. *Audiology*, **90**, 99–113.
- Gradshteyn, I. S. and Ryzhik, I. M. (1980) *Table of Integrals, Series, and Products*. Boston: Elsevier Academic Press.
- Kato, S., Mastrantonio, G. and Ishikawa, M. (1925) An interpretable family of projected normal distributions and a related copula model for bayesian analysis of hypertoroidal data. *arXiv*.
- Kendall, D. G. (1974) Pole-seeking brownian motion and bird navigation. *Journal of the Royal Statistical Society: Series B (Methodological)*, **36**, 365–417.
- Kent, J. T. and Mardia, K. V. (2022) *Spatial Analysis*. Wiley.
- Kent, J. T., Mardia, K. V. and Rao, J. S. (1979) A characterization of the uniform distribution on the circle. *The Annals of Statistics*, **7**, 882–889.
- Mardia, K. V. (1972) *Statistics of Directional Data*. Academic Press, London.
- (1975a) Statistics of directional data (with discussion). *Journal of Royal Statistical Society B*, **37**, 349–393.
- (1975b) Characterizations of directional distributions. In G. P. Patil, S. Kotz and J. K. Ord (eds), *Statistical Distributions in Scientific Work*, **3**, 365–385 Reidel, Dordrecht.
- (2017) *The magic of score matching estimators and approximations for distributions on manifolds and some cutting edge applications to molecular biology*. Proceedings of 61th ISI World Statistics Congresses, Marrakech.
- (2018) *A new breakthrough in the estimation methodology for standard directional distributions*. Proceedings of the 20th International Conference on Information Fusion, IEEE, Cambridge.
- Mardia, K. V. and Jupp, P. E. (2000) *Directional Statistics*. Wiley.
- Mathewson, K. E., Gratton, G., Fabiani, M., Beck, D. M. and Ro, T. (2009) Rescuing stimuli from invisibility: Induced alpha phase determines visual awareness. *Journal of Neuroscience*, **29**, 2725–2732.
- Mushtaq, F., Welke, D., Gallagher, A., Pavlov, Y. G. et al. (2024) One hundred years of eeg for brain and behaviour research. *Nature Human Behaviour*, **8**, 405–419. URL: <https://www.nature.com/articles/s41562-024-01941-5>.
- Muthuswamy, J. (2004) Biomedical signal analysis. In Kutz, M (eds) *Standard Handbook of Biomedical Engineering and Design.*, **14**, 1–18.

- Muthuswamy, J. and Thakor, N. V. (1998) Spectral analysis of neurological signals. *Journal of Neuroscience Methods*, **83**, 1–14.
- Notbohm, A. and Herrmann, C. S. (2016) Flicker regularity is crucial for entrainment of alpha oscillations. *Frontiers in Human Neuroscience*, **10**, 444.
- Nuñez-Antonio, G. and Gutiérrez-Peña, E. (2005) A bayesian analysis of directional data using the projected normal distribution. *Journal of Applied Statistics*, **32**, 995–1001.
- Presnell, B. P., Morrison, S. P. and Littell, C. (1998) Projected multivariate linear model for directional data. *Journal of the American Statistical Association*, **93**, 1068–1077.
- Miranda de Sá, A. M. F. L. and Felix, L. B. (2003) Multi-channel evoked response detection using only phase information. *Journal of Neuroscience Methods*, **129**, 1–10.
- Miranda de Sá, A. M. F. L., Infantosi, A. C. and M., S. D. (2002) Coherence between one random and one periodical signal for measuring the strength of responses in the electroencephalogram during sensory stimulation. *Medical and Biological Engineering and Computing*, **40**, 99–104.
- Stephens, M. A. (1969) Tests for the von Mises distribution. *Biometrika*, **56**, 149–160.
- Subasi, A. (2019) Biomedical signal analysis and its usage in healthcare. In Paul, S. (eds) *Biomedical Engineering and its Applications in Healthcare.*, **14**, 423–452.
- Watson, G. S. (1983) *Statistics on Spheres*. John Wiley & Sons.

## A Appendix 1: Deeper Examination of the EEG Model

We give a full characterization of the EEG model outlined for flash stimulation in Section 2 using the fundamentals of signal processing and impulse trains. This characterization is implicit in the literature but has not been reported in any publication.

The intermittent photic stimulation produced by flashes (used in the application in Section 8 can be modeled as a periodic impulse train (an evenly spaced series of Dirac delta functions). If the time between consecutive impulses is  $T$ , then  $T$  is the stimulation period and the stimulation frequency is  $f_0 = 1/T$ .

The Fourier transform of a periodic impulse train is another impulse train in the frequency domain with impulses located at integer multiples of the fundamental frequency  $f_0$  (see below). For example, stimulation at 6 Hz corresponds to  $T = 1/6$  s (six flashes per second) and produces spectral impulses spaced by 6 Hz. That is, the spectrum

contains impulses at integer multiples of the fundamental frequency  $f_0 = 1/T$ . Figure 10 shows impulse train (Dirac deltas) with spacing  $T$  (in Left) in time domain and its corresponding impulse train with spacing  $1/T$  in frequency domain (in Right). Both are impulse trains.



Figure 10: Left: impulse train (Dirac deltas) with spacing  $T$ . Right: magnitude of its discrete Fourier transform showing spectral impulses with spacing  $1/T$ .

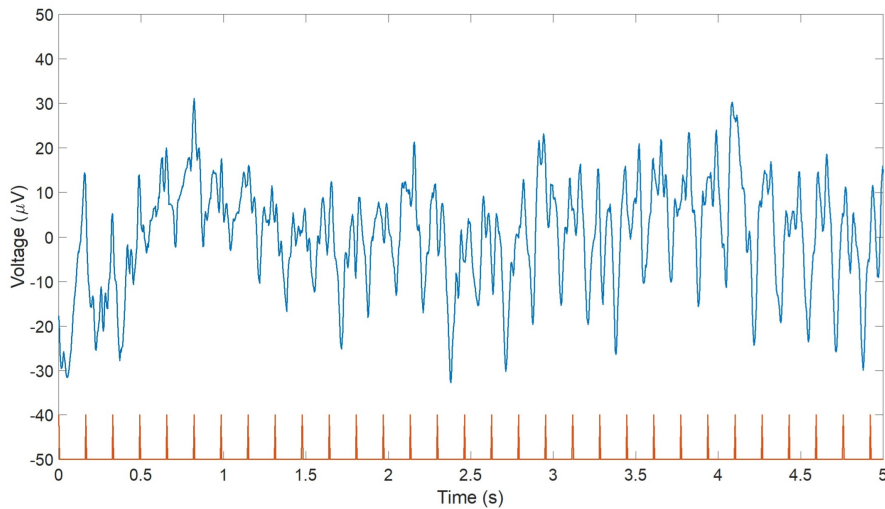


Figure 11: Five-second EEG time series from a 13-year-old subject recorded at electrode O1 during 6 Hz photic stimulation. Red marks indicate stimulus times.

## A.1 Impulse trains and the additive linear error model

We now give more details of the output relevant to our EEG application of Section 8.8. Figure 11 shows a five-second EEG time series from a 13-year-old subject recorded at electrode O1 during 6 Hz photic stimulation where red marks indicate stimulus times at time at the step of  $1/6$  seconds. The corresponding Figure 12 shows the magnitude of the discrete Fourier transform of the 5-second EEG segment where the vertical lines mark the stimulation frequency (6 Hz) and its harmonics.

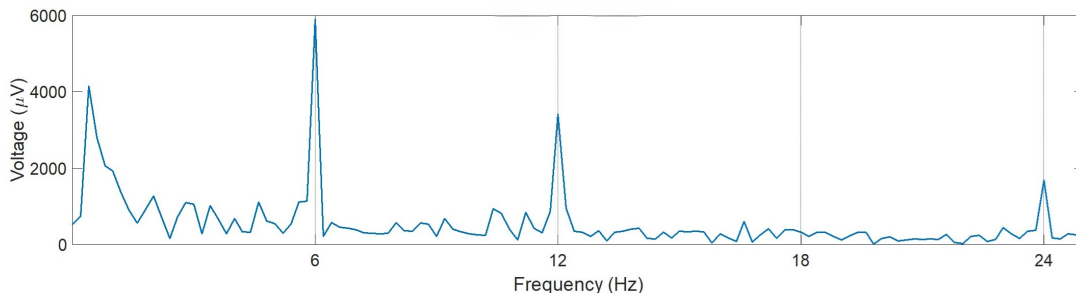


Figure 12: Magnitude of the discrete Fourier transform of the 5-second EEG segment. Vertical lines mark the stimulation frequency (6 Hz) and its harmonics.

**Deterministic Impulse Train** An ideal continuous-time impulse train with period  $T$  in the **time domain** is

$$s(t) = \sum_{n=-\infty}^{\infty} A_n \delta(t - nT), \quad (\text{A.1})$$

where  $\delta(\cdot)$  is the Dirac delta,  $A_n$  is the amplitude of the  $n$ -th impulse (constant or random), and impulses occur at  $t = nT$ . In the **frequency domain**, the Fourier transform of  $s(t)$  is a comb of impulses:

$$S(f) = \frac{1}{T} \sum_{k=-\infty}^{\infty} A_k \delta\left(f - \frac{k}{T}\right), \quad (\text{A.2})$$

where  $f$  is the frequency.

### Additive error model: linear input-output system

We model the observed signal (output) as the impulse train (input) corrupted by additive noise:

$$x(t) = s(t) + \varepsilon(t), \quad (\text{A.3})$$

where  $\varepsilon(t)$  is additive Gaussian noise with  $\varepsilon(t) \sim \mathcal{N}(\mu, \sigma^2)$  (applied point-wise in time). In **frequency-domain**, taking Fourier transforms gives

$$Y(f) = S(f) + N(f) \quad (\text{A.4})$$

where  $N(f)$  is complex Gaussian noise,  $N(f) \sim \mathcal{CN}(\mu_N, \sigma_N^2)$ . The real and imaginary parts of  $N(f)$  are independent normals:  $\text{Re } N(f), \text{Im } N(f) \sim \mathcal{N}(\mu_N, \sigma_N^2)$ . The model (A.4) given at (1.1) with its discrete Fourier representation and  $S(f)$  with deterministic amplitude  $\mu$  at a given frequency.

**Signal-to-Noise Ratio** Define frequency-specific SNR as

$$\text{SNR}(f) = \frac{\mathbb{E}[|S(f)|^2]}{\mathbb{E}[|N(f)|^2]}.$$

For complex Gaussian noise with variance  $\sigma_N^2$  per real component,  $\mathbb{E}[|N(f)|^2] = 2\sigma_N^2$ , so

$$\text{SNR}(f) = \frac{\mathbb{E}[|S(f)|^2]}{2\sigma_N^2}.$$

With  $S(f) = \mu$  at a given frequency, this reduces to

$$\text{SNR}(f) = \mu^2 / (2\sigma_N^2), \quad (\text{A.5})$$

which is the SNR value (2.4) .

## A.2 Phase angles of EEG in flash stimulation

This impulse–train plus noise model captures the principal features of photic stimulation in EEG: a comb-like spectrum at the stimulation frequency and its harmonics, superimposed on broadband noise that can mask or distort the spectral peaks. The model is therefore useful for simulation, for understanding the spectral signatures of stimulation, and for designing detection or filtering strategies based on SNR. Flashes interact with the brain’s ongoing rhythms in a time-specific manner: the instantaneous phase of an oscillation at stimulus onset determines neuronal excitability, making phase measurements essential for explaining and predicting the neural and perceptual effects of brief visual stimuli (Busch et al., 2009; Busch and VanRullen, 2010). Furthermore, Notbohm and Herrmann (Notbohm and Herrmann, 2016), together with Mathewson et al. (Mathewson et al., 2009), provide compelling evidence that the brain’s responsiveness to visual flash stimulation is governed primarily by the phase of ongoing oscillations—far more than by their amplitude—demonstrating that phase alignment at stimulus onset determines both the strength of neural entrainment and the likelihood of conscious perceptual awareness. Thus, to sum up, the PIN distribution for the phase-angle data in Section ?? is appropriate.

## A.3 Origin of CSM

We now discuss the model given by (A.3) in the discrete time domain and its corresponding Fourier representation (A.4) in the discrete Fourier domain and recast the method of Friedman et al. (1984) into a model framework. Below we give a representation for the observed EEG (in time domain and frequency domain) and show how the phase statistics used by Friedman et al. (1984) lead naturally to the CSM measure.

Assume a real-valued discrete time series  $x(t)$ ,  $t = 1, \dots, n$ , with  $n$  even corresponding to (A.3). A convenient finite Fourier series representation that isolates the sinusoidal components is

$$x(t) = b_0 + \sum_{j=1}^{n/2-1} [a_j \sin(2\pi jt/n) + b_j \cos(2\pi jt/n)] + b_{n/2} \cos(\pi t), \quad (\text{A.6})$$

where the coefficients  $\{a_j, b_j\}$  determine the contribution at each Fourier frequency. We model the coefficients at a given frequency  $j$  as

$$Y_j = a_j + ib_j = r_j e^{i\theta_j}, \quad (\text{A.7})$$

the phase  $\theta_j$  is then a circular random variable whose distribution under the signal-plus-noise model is the PIN model used in our theoretical development. Friedman et al. (1984) focused on the  $\bar{R}^2$  or CSM (using sample circular variance as  $1 - \bar{R}^2$  but not the standard variance  $1 - \bar{R}$ ) computed from the collection of phase angles  $\{\theta_j\}$ . The CSM statistic measures phase synchrony (concentration) across trials or channels for a given Fourier coefficient and is therefore useful as a criterion for distinguishing signal from uniform (noise) phase distributions.

In our implementation, we compute the discrete Fourier transform of the discretized EEG  $x(t)$ ,

$$Y_j = r_j e^{i\theta_j} = \sum_{t=1}^n x(t) e^{-i2\pi jt/n}, \quad j = 1, \dots, n, \quad (\text{A.8})$$

and then obtain  $\bar{R}^2$  (CSM) from the phases  $\{\theta_j\}$  at the frequency of interest.

**Remark.** As a validation of the PIN approximation, the empirical behaviour of the observed resultant for EEG data closely matches the theoretical distribution under the PIN model; see Miranda de Sá and Felix (2003) for related results.

## B Appendix 2: Moments

We now give a proof of the moment formulae (3.3) and (3.4). Without loss of generality, in our model (2.1) we take  $\sigma = 1$  and  $\mu_1 = 2\sqrt{\gamma}$ ,  $\mu_2 = 0$ . Then the joint density of  $(r, \theta)$  in (2.1) is

$$f(r, \theta; \gamma) = \frac{\exp(-2\gamma)}{2\pi} r \exp(-r^2/2) \exp\{2\sqrt{\gamma} r \cos \theta\}. \quad (\text{B.1})$$

Hence,

$$E(\sin p\theta) = \frac{\exp(-2\gamma)}{2\pi} \int_0^\infty r \exp(-r^2/2) a_1(r) dr, \quad (\text{B.2})$$

where

$$a_1(r) = \int_0^{2\pi} (\sin p\theta) \exp\{2\sqrt{\gamma} r \cos \theta\} d\theta. \quad (\text{B.3})$$

The integrand in  $a_1(r)$  is an odd function of  $\theta$ , so  $a_1(r) = 0$ . This proves (3.3).

To prove (3.4), note that

$$E(\cos p\theta) = \exp(-2\gamma) \int_0^\infty r \exp(-r^2/2) a_2(r) dr, \quad (\text{B.4})$$

where

$$a_2(r) = \frac{1}{2\pi} \int_0^{2\pi} (\cos p\theta) \exp\{2\sqrt{\gamma} r \cos \theta\} d\theta. \quad (\text{B.5})$$

From Appendix 1 of Mardia and Jupp (2000),

$$a_2(r) = I_p(2\sqrt{\gamma} r). \quad (\text{B.6})$$

Using Gradshteyn and Ryzhik (1980), formula 6.631(7), p. 706,

$$\int_0^\infty r \exp(-r^2/2) I_p(2\sqrt{\gamma} r) dr = \sqrt{\frac{\pi\gamma}{2}} \exp(\gamma) \{I_{(p-1)/2}(\gamma) + I_{(p+1)/2}(\gamma)\}. \quad (\text{B.7})$$

Substituting (B.6) and (B.7) into (B.4) yields (3.4).

## C Appendix 3: Assessment of Approx 1 and Approx 2

We now give some more comparisons of Approx 1 and Approx 2 of Section 3. Table

Table 3: Von Mises approximations to PIN( $\gamma$ ); for given  $\gamma$ ,  $\kappa_1$  from Approx 1 and  $\kappa_2$  from Approx 2.

$\gamma$	$\kappa_1$	$\kappa_2$
0.05	0.5686	0.5746
0.25	1.3513	1.4161
0.50	2.0786	2.2473
0.75	2.7936	3.0642
1.00	3.5628	3.9059
2.00	7.2644	7.5655
2.50	9.2872	9.5093
3.75	14.3748	14.4765
5.00	19.4204	19.4790

3 gives the concentration parameters  $\kappa$  for Approx 1 and Approx 2 ( $\kappa_1$  and  $\kappa_2$  respectively) to  $\gamma$  of the PIN distribution. From this table, we see that  $\kappa_2 \geq \kappa_1$  for the values shown, so the difference  $\kappa_2 - \kappa_1$  is nonnegative. Further, the maximum difference is approximately 0.37 near  $\gamma \approx 2.5$ ; for very small and very large  $\gamma$  the two approximations coincide to numerical precision. Figure 13 plots the difference between the two approximations; the largest discrepancy occurs in the moderate SNR range. Values are nonnegative as again confirming  $\kappa_2 \geq \kappa_1$ . Figure 14 compares the two von Mises approximations (Approx 1, Approx 2) to the PIN density for SNR values 1, 1.5, 2 and 4 where one expects to see the larger differences. Approx 2 is slightly closer to the PIN in the intermediate SNR range (roughly 0.75–2), likely because it incorporates the second trigonometric moment.

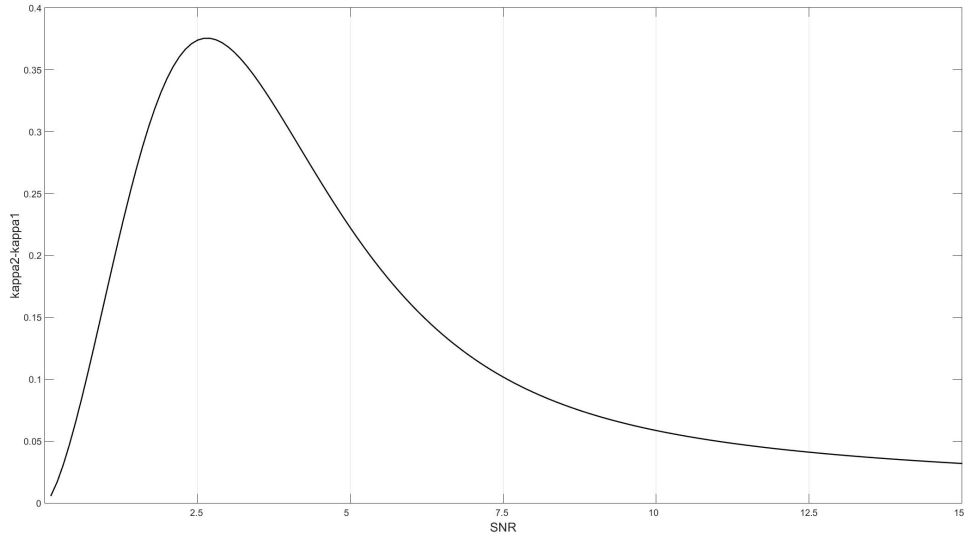


Figure 13: Difference  $\kappa_2 - \kappa_1$  as a function of SNR (where  $\text{SNR}=2\gamma$ ).

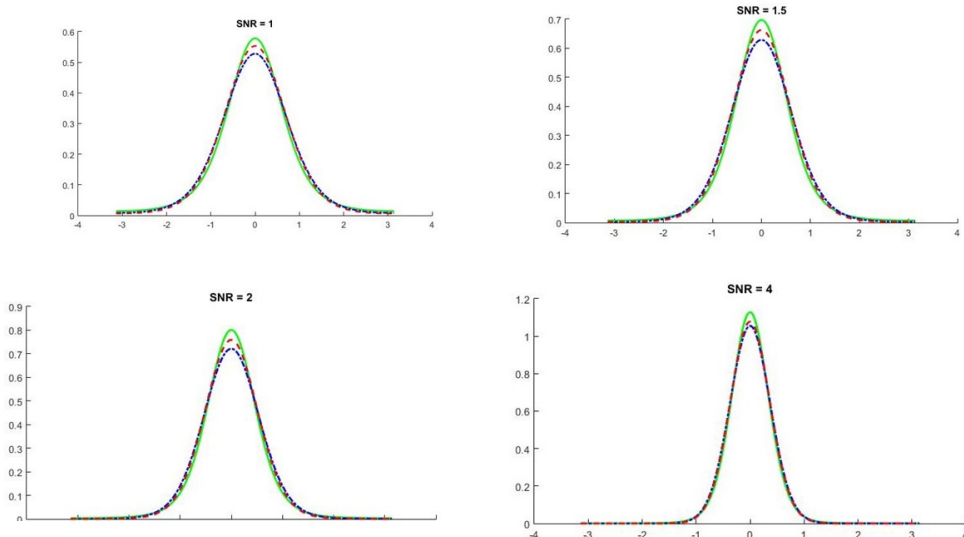


Figure 14: Comparison of PIN density (solid green) with von Mises Approx 1 (dashed blue) and Approx 2 (dashed red) for some selected SNR values.

## Kullback–Leibler comparison

We assessed the two approximations using Kullback–Leibler (KL) divergence from the PIN density. The KL differences between Approx 1 and Approx 2 are negligible: the largest observed difference is about 0.003 at  $\gamma = 0.75$ , with Approx 1 being marginally better. Thus we note that:

- Approx 1 is a well-established choice and performs slightly better in some tail

regions.

- Approx 2 is algebraically simpler and accounts for higher trigonometric moments, improving fit in the moderate SNR range.
- For practical purposes (e.g., thresholding  $\bar{R}$  in applications), the two approximations give nearly identical results; differences are most relevant only in the extreme tails.